PCCP

PAPER

View Article Online
View Journal | View Issue

Cite this: *Phys. Chem. Chem. Phys.*, 2025, **27**, 20177

Systematic growth of non-epitaxial ZnO shell over Ln^{3+}–Li^{+} co-doped Y_2O_3 phosphor core

Shefali Jayswal *[ab] and Rakesh S. Moirangthem [bc]

Here, Ln^{3+}–Li^{+} co-doped Y_2O_3@ZnO core–shell heterostructures were synthesized by three different techniques – intermediate layer conversion method, a hydrothermal method, and an interlayer mediated hydrothermal method. The synthesis procedure is optimized based on the thickness and compactness of the developed shell. The growth kinetics and synthesis mechanism of each adopted method have been explained in detail using XRD, FESEM, TEM, SAED, and EDX characterization techniques. The interlayer-mediated hydrothermal method proved to be the best technique for developing a thin, compact layer of ZnO shell on the upconversion microsphere, but only up to a critical thickness. Optimization of the shell thickness was done to understand the role of the magnitude and sign of lattice strain in the core–shell design. Conformal ZnO shell growth on the upconversion core was possible only for a small volume of the precursor solution, as anisotropic structures started to appear in the solution for larger volumes.

Received 13th January 2025,
Accepted 10th August 2025

DOI: 10.1039/d5cp00156k

rsc.li/pccp

1. Introduction

Multicomponent core–shell heterostructures are hybrid materials where one material (the core) is encapsulated within another type (the shell). This hybrid structure combines the advantages and overcomes the weaknesses of the individual components, enhancing performance and generating new functionalities.[1–4] Lanthanide-doped upconversion phosphors are an emerging class of materials that can convert NIR photons to UV-Visible photons through a multiphoton absorption and relaxation process.[5] Upconversion nanoparticles (UCNPs) have enormous potential for bioscience applications; however, further development is required to optimize the optical characteristics of these upconversion phosphors for future commercialization. Growing a shell with comparable lattice constants around the core has been found to improve the upconversion emission significantly. The shell can shield the luminescent lanthanide ions in the core, particularly those close to the surface, from both vibrational deactivation from solvents or surface-bound ligands in the case of colloidal dispersions, as well as from nonradiative decay brought on by surface defects.[6–8] Core–shell heterostructures formed between upconversion phosphors and semiconductors have drawn great interest over the past few decades. The semiconductor shell utilizes the visible radiation emitted by the upconversion phosphors *via* the FRET/radiation-reabsorption mechanism, and thereby produce reactive oxygen species for its use in photodynamic therapy,[9,10] photocatalysis,[11,12] photovoltaics,[13] and energy storage applications.[12,14] The properties of the core–shell heterostructure depend on its composition, structure, crystal phase, exposed facet, spatial organization, and the interfacial strain between the components.[15,16] In general, epitaxial growth of the shell over the core is preferred when designing the core–shell heterostructure. However, in our case, the presence of a high degree of lattice mismatch between upconversion phosphor and semiconductor crystals makes it a formidable challenge to form a conformal core–shell heterostructure.[17,18] The interfacial strain between two lattice mismatched crystals causes the growth of the shell layer only up to a specific thickness, causing shape inhomogeneity and the development of anisotropic structures beyond it due to strain relaxation.[15,19,20] Several strategies, such as chemical vapor deposition, electrospinning, chemical reduction, colloidal synthesis, self-assembly, hydrothermal, and solvothermal methods, have been used earlier to design high-quality UCNPs@semiconductor core–shell heterostructures.[1,15,21,22] However, a few articles, like this, are dedicated to outlining the various synthetic methods for the efficient growth of a lattice mismatched ZnO shell onto a well-known upconversion phosphor-Ln^{3+}–Li^{+} co-doped Y_2O_3. The doping of lithium ions is done to increase the efficiency of upconversion emission by relaxing the conditions of parity forbidden f–f transitions of lanthanide ions. This work also explains the role of interfacial strain in getting a conformal and coherent core–shell heterostructure.

---

[a] *Department of Physics, Manipal Institute of Technology Bengaluru, Manipal Academy of Higher Education, Manipal, India. E-mail: shefali.jayswal@manipal.edu, jayswal.shefali106@gmail.com*

[b] *Department of Physics, Indian Institute of Technology (ISM) Dhanbad, Jharkhand-826004, India*

[c] *Department of Physics, Manipur University, Canchipur, Imphal-795003, Manipur, India. E-mail: rakesh@manipuruniv.ac.in*

2. Experimental details

2.1. Materials

Yttrium nitrate hexahydrate ($Y(NO_3)_3{\cdot}6H_2O$), sodium acetate anhydrous (CH_3COONa), ytterbium nitrate pentahydrate ($Yb(NO_3)_3{\cdot}5H_2O$), erbium nitrate pentahydrate ($Er\ (NO_3)_3{\cdot}5H_2O$), thulium nitrate pentahydrate ($Tm(NO_3)_3{\cdot}5H_2O$), lithium nitrate ($LiNO_3$), zinc nitrate hexahydrate ($Zn(NO_3)_2{\cdot}6H_2O$) and polyvinylpyrrolidone (PVP-40, average molecular weight-40 000) ($(C_6H_9NO)_n$) were purchased from Sigma-Aldrich, India and used as procured. Ethylene glycol ($C_2H_6O_2$), and hexamethylenetetramine (HMTA, $C_6H_{12}N_4$) were purchased from Merck and were used as received. Deionized (DI) water used in the experiments were obtained from the Milli-Q system (Millipore).

2.2. Synthesis of Ln^{3+}–Li^{+} co-doped Y_2O_3 microspheres

YYTEL (3 mol% Yb^{3+}–0.2 mol% Er^{3+}–0.5 mol% Tm^{3+}–2 mol% Li^{+} co-doped Y_2O_3) phosphor microspheres were synthesized using an earlier reported procedure by our group.[12,23]

2.3. Synthesis of a YYETL@ZnO core–shell by the interlayer conversion method

To coat an amorphous interlayer of AA-$[Zn(OH)_4]^{2-}$ over YYETL microspheres,[22,24] they were functionalized with CTAB molecules in an aqueous medium and kept aside. Then, 0.3 mmol of CTAB and 0.2 mmol of ascorbic acid were dissolved in a 50 ml aqueous solution, and to it, 1 mmol of $Zn(NO_3)_2{\cdot}6H_2O$ and HMTA were added under constant stirring. After that, 10 ml of the functionalized YYETL microspheres were added drop-by-drop to the above mixture and heated at 85 °C for 10 hours under continuous stirring. This resulted in the formation of YYETL@AA-$[Zn(OH)_4]^{2-}$ microspheres, which were collected after washing with DI water and ethanol. The final products were obtained by calcination at 350 °C for 2h, which decomposes zinc hydroxide into ZnO and forms YYETL@ZnO microspheres (Fig. 1a). It is denoted as YYETL@ZnO-I throughout this work. Functionalization of YYETL microspheres with CTAB is done for two reasons: first, to make it hydrophilic and, second, to make it act as a template for the growth of the amorphous shell on the microsphere surface. Ascorbic acid and Zn^{2+} ions create the AA-Zn(II) complex, which is converted to AA-$[Zn(OH)_4]^{2-}$ by the addition of HMTA.

2.4. Synthesis of a YYETL@ZnO core–shell by the hydrothermal method

Here, the hydrothermal method is used to grow ZnO nanoparticles on the surface of YYETL microspheres *via* electrostatic attraction (Fig. 1b). 27 mg of YYETL phosphors were dispersed in 50 mL of DI water, and an equimolar ratio of zinc nitrate hexahydrate (0.5 mM) and HMTA was added to it and heated at 95 °C for 4 h under continuous stirring. After cooling, YYETL@ZnO microspheres were obtained by washing the sample with DI water and ethanol and drying it at 60 °C. They are denoted as YYETL@ZnO-II in this work.

2.5. Synthesis of a YYETL@ZnO core–shell by the interlayer mediated hydrothermal method

In this method[25] (Fig. 1c), YYETL microspheres were functionalized with PVP, a non-toxic water-soluble polymer. 0.6 g of PVP

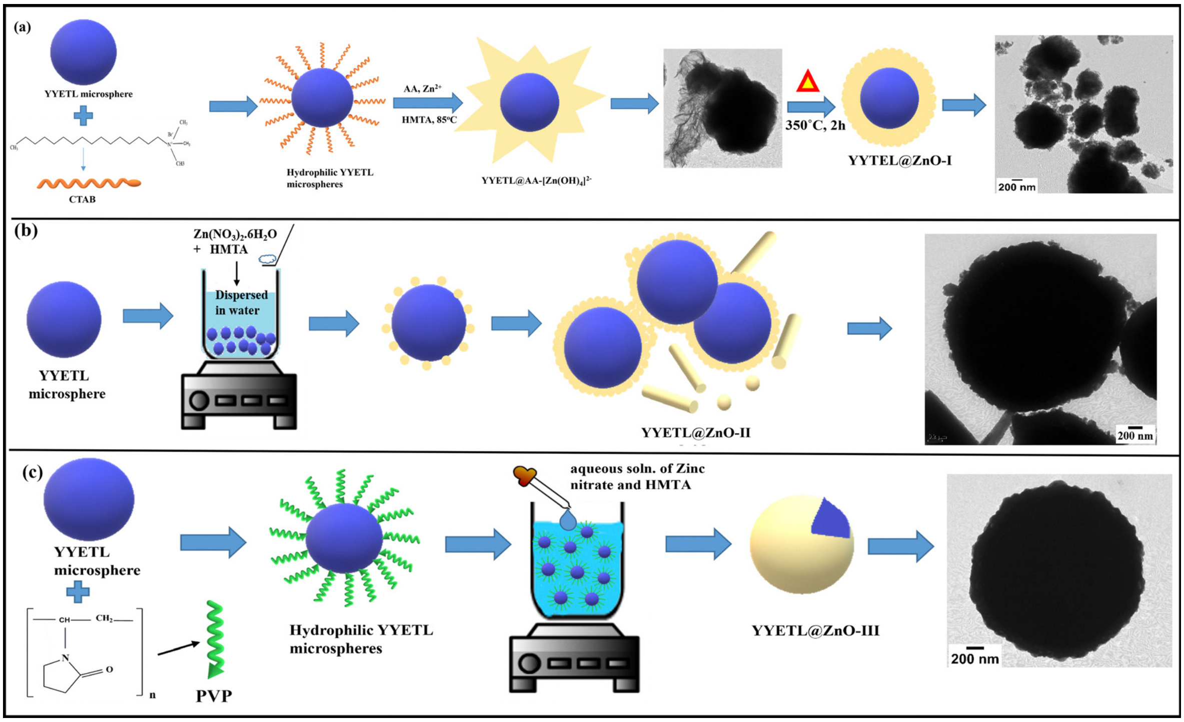

Fig. 1 Schematic representation of the synthesis procedures followed to grow ZnO shell on YYETL microspheres by (a) interlayer conversion method, (b) hydrothermal method, and (c) interlayer mediated hydrothermal method.

was added to 50 mL of water, and 75 mg of the YYETL microspheres were added to it and stirred for 20 min. Then, '*x*' mL aqueous solution of 0.1 M HMTA and $Zn(NO_3)_2 \cdot 6H_2O$ were subsequently added and stirred for 4 h at 95 °C. The as-obtained products were centrifuged and washed with DI water and ethanol, then dried at 60 °C. It is denoted as YYETL@ZnO-III-*x* in this work, where x = 0.5 mL and 1.5 mL, is the volume of the precursor solution used for ZnO shell growth.

2.6. Characterization

The X-ray diffraction (XRD) pattern was recorded using a PANalytical X'pert Pro diffractometer in the range of $2\theta = 10^\circ$ to 70° with CuKα ($\lambda = 1.542$ Å) as the radiation source. The Field Emission Scanning Electron Microscopy (FESEM) images were obtained using the FEI Nova NanoSEM 450 instrument. The elemental distribution was studied with E-SEM (FEI model Quanta 200 3D) equipped with an Energy-Dispersive X-ray spectroscopy (EDX) attachment. The morphology and SAED pattern were obtained using a Transmission Electron Microscope (FEI TECNAI T20 ST) operated at 200 kV. HRTEM (High Resolution TEM) and HAADF-STEM (High-Angle Annular Dark-Field Scanning Transmission Electron Microscopy) images and elemental mapping data were obtained using a Transmission Electron Microscope (JEOL JEM F200) operated at 200 kV. The samples for TEM and HRTEM analysis were prepared by dispersing a small amount of powder in ethanol and drop-casting it on a carbon-coated copper grid. The upconversion emission photoluminescence (UCPL) spectra were recorded on an SP2300 grating spectrograph (Princeton Instruments, USA) using a 980 nm continuous wave (CW) diode laser as the excitation source. The laser power was measured through a power meter (Model S310C, Thorlabs, USA). All the upconversion emission spectra were recorded at a power of 2.09 W. The lattice parameters of YYETL and ZnO were calculated from XRD data using UnitCellWin software.

3. Results and discussion

The design and growth of YYETL@ZnO core–shell heterostructures were done *via* three different methods and their results are evaluated *via* FESEM, TEM, EDX, and SAED/XRD characterization techniques. The quality of the developed shell is evaluated based on factors like uniformity, compactness, and thickness as most upconversion core–shell heterostructures require an optimum shell thickness for all their applications. The lattice mismatch between YYETL and ZnO can be calculated using the formulae:[26]

$$f = \frac{\alpha_{\text{core}} - \alpha_{\text{shell}}}{\alpha_{\text{core}}}$$

where α is the lattice constant of the unit cell. The value of lattice mismatch '*f*' between cubic YYETL (lattice constant = 10.595 Å) and hexagonal ZnO (lattice constant = 3.250 Å) is +0.6932, obtained using the above formulae. The lattice mismatch is +69.32%, which is much higher than the minimum allowed value of lattice strain for growing an epitaxial shell. The nominal criterion of lattice mismatch to be $<2\%$ is necessary to minimize the interfacial energy of the hybrid materials and develop a thick shell. So, designing a core–shell heterostructure with two highly lattice-mismatched materials remains a significant challenge.

The motive behind the use of three different methods to synthesize the core–shell heterostructure is to optimize the synthesis procedure to develop a conformal and coherent core–shell heterostructure between two lattice mismatched crystals with a high '*f*' value. This work outlines the controlled synthesis of a core–shell heterostructure between two different semiconductor crystals by introducing different amorphous interlayers. It underscores the role played by the PVP interlayer in acting as a bridge between two materials with a high value of '*f*'. In its absence, it is hard to get a conformal core–shell heterostructure with an optimum shell thickness. The three synthesis methods have been assessed on factors like the quality of the developed ZnO shell and their ease of synthesis. It also highlights the role of interfacial strain and how it allows the growth of the overlayer only up to a critical thickness, as beyond it, dislocation defects relax the misfit strain, resulting in the formation of free ZnO nanostructures in solution.[27]

Fig. 2(a) and (b) show the FESEM and TEM images of the YYETL phosphor microspheres, depicting the formation of a compact and dense structure *via* the self-assembly of nanoparticles. Fig. 2(c) illustrates the EDX spectra of the YYETL microspheres, which depict the presence of yttrium, oxygen, ytterbium, erbium, and thulium elements. Carbon comes from carbon tapes used to mount the sample on stubs for characterization. The lithium element is not detected in the EDX spectra due to its low atomic weight and low energy. SAED patterns are diffraction spots of crystal planes in reciprocal space. The SAED pattern in Fig. 2(d) indicates the polycrystalline nature of the sample with bright diffraction spots corresponding to the (222), (400), (440), (622) and (822) planes of cubic Y_2O_3 (JCPDS card no. 25-1200). Due to their low concentration, no prominent oxide peaks of doped lanthanide ions are seen in the SAED pattern. It also confirms these dopants' inclusion at the Y^{3+} site *via* substitution.

Fig. 3(a) shows the TEM micrographs of YYETL@AA-$[Zn(OH)_4]^{2-}$ complex core–shell heterostructures prepared by the interlayer conversion method. The amorphous intermediate layer of AA-$[Zn(OH)_4]^{2-}$ is grown to overcome the significant lattice mismatch between the YYETL core and ZnO semiconductor in forming the core–shell heterostructures.[22] A closer look reveals a clear contrast between the crystalline YYETL core and the uneven amorphous layer of the AA-$[Zn(OH)_4]^{2-}$ composite. The SAED pattern in Fig. 3(b) further confirms the formation of a dense amorphous layer of zinc hydroxide on it with its diffuse diffraction rings indexed to the (132), (402), and (211) planes of the orthorhombic crystal structure of $Zn(OH)_2$ (JCPDS 038-0385). On annealing at 350 °C, the AA-$[Zn(OH)_4]^{2-}$ complex decomposes to form ZnO nanoparticles (Fig. 3c). The amorphous layers on the outside have transformed after calcination into a layer comprising ZnO nanoparticles. The EDX pattern (Fig. 3d) collected from the YYETL@ZnO-I microspheres gives

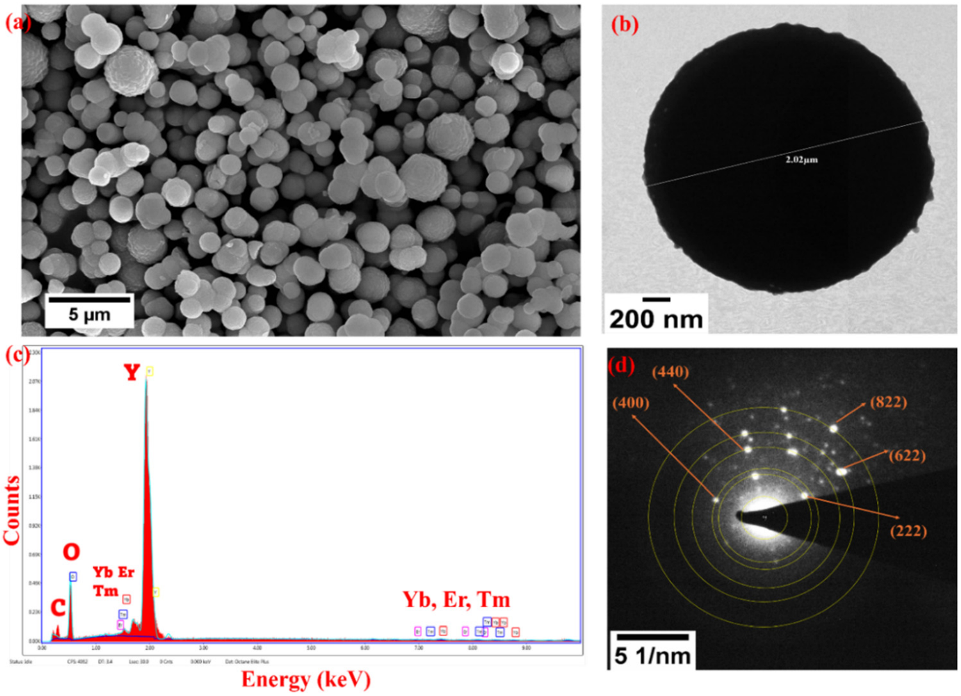

Fig. 2 (a) FESEM image, (b) TEM image, (c) EDX and (d) SAED pattern of the YYETL microspheres.

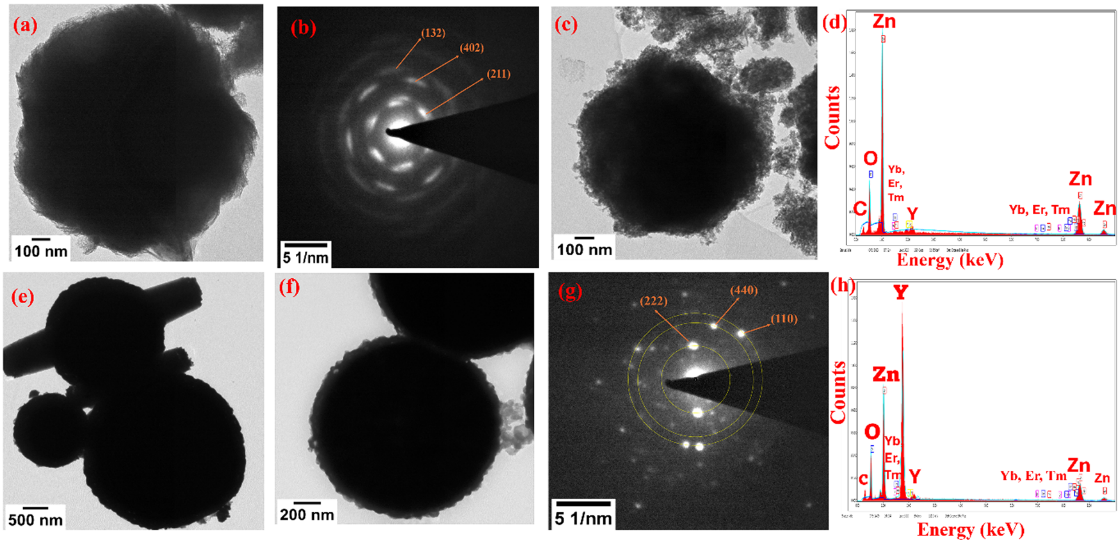

Fig. 3 (a) TEM image and (b) SAED pattern of the YYETL@AA-$[Zn(OH)_4]^{2-}$ complex core–shell heterostructure, (c) TEM image and (d) EDX pattern of the YYETL@ZnO-I microspheres, (e and f) TEM images, (g) SAED and (h) EDX pattern of the YYETL-ZnO-II microspheres.

major counts from zinc and oxygen atoms with a minimal signal from yttrium atoms and doped lanthanide ions due to the thick ZnO shell masking the whole core. Thus, we can conclude that the intermediate layer conversion method results in a thick coating of ZnO around the YYETL core, which is not ideal for transmitting NIR light to the phosphor core. Thin shell growth is necessary for an efficient photon upconversion process, and it is used by the semiconductor shell for various applications.[28] Furthermore, this method leads to wild and unattended growth into the solution medium, forming many clustered ZnO nanoparticles in the solution apart from those on the core YYETL microspheres, which is a significant disadvantage for application purposes. Fig. 3(e) and (f) show the TEM images of YYETL@ZnO-II microspheres synthesized *via* the hydrothermal method without using an intermediate layer. This technique resulted in thin, non-uniform shell deposition around the core microspheres, with clustered deposition of ZnO nanoparticles at certain facets and the formation of free ZnO micro/nanorods in the solution. Formation of discrete islands of the ZnO shell on the core upconversion phosphors is due to the Volmer–Weber model of epitaxial growth.[19,26] It also proves that the current method cannot exploit all the Zn^{2+} ions for attaching onto the surface of the YYETL microspheres. As a result, many free Zn^{2+} ions remain in the solution and, after reacting with HMTA, lead to the emergence of loose ZnO microstructures. This could also be due to the significant lattice mismatch between the YYETL and ZnO semiconductors, which prevents deposition *via* nucleation of ZnO onto YYETL. In addition, the microspheres remain aggregated in solution due to the lack of chemical forces acting as a 'dispersant' between them. So, the second process gave us the desired results of developing a thin shell around the core with few discrepancies like the appearance of loose ZnO microrods, clustered deposition of ZnO nanoparticles at certain facets, and aggregation of YYETL microspheres. The bright diffraction spots in the SAED pattern (Fig. 3g) of the YYETL@ZnO-II microspheres can be indexed to the (222) and (440) planes of cubic Y_2O_3 and (110) planes of hexagonal ZnO. The EDX spectra (Fig. 3h) corroborate the presence of yttrium, zinc, oxygen, ytterbium, erbium, and thulium elements in the heterostructure. The major count from the yttrium element depicts that the ZnO shell does not entirely mask the core, and thereby an optimum shell transmittance is present.

Fig. 4(a)–(d) exhibit the FESEM and TEM images of the YYETL@ZnO-III-*x* microspheres prepared by the interlayer mediated method. Here, PVP is used as an interlayer, acting as a surface functionalizing agent and an aid in nanoparticle synthesis.[29] It contains hydrophilic (pyrrolidone moiety) and hydrophobic (the alkyl group) components. As no lattice mismatch exists between a crystal and an amorphous layer, the PVP macromolecule is introduced as the amorphous layer to eliminate the high lattice mismatch between YYETL and ZnO.[30] Due to the high molecular weight of PVP used here (K40), they possess a long chain length and act as a dispersant between two particles. It prevents nanoparticle aggregation by using repulsive forces generated by hydrophobic carbon chains that extend into the solvent and interact with one another (steric hindrance effect).[31] The Zn^{2+} cations connect to the negatively charged $C{-}O^-$ group in PVP and progressively change to ZnO by interaction with OH^- released from HMTA. As the growth rate of ZnO is high in basic media, we employ HMTA as the base source to provide a weak basic environment for regulated ZnO nanocrystal growth.[32,33] The slow release and nucleation of metal ions are beneficial to the formation of a compact core–shell heterostructure. The TEM image (Fig. 4a) of YYETL-ZnO-III-0.5 microspheres depicts the coating of a thin and compact heterogeneous layer of the ZnO shell all over the YYETL core, with no appearance of any loose ZnO nanostructures in solution.

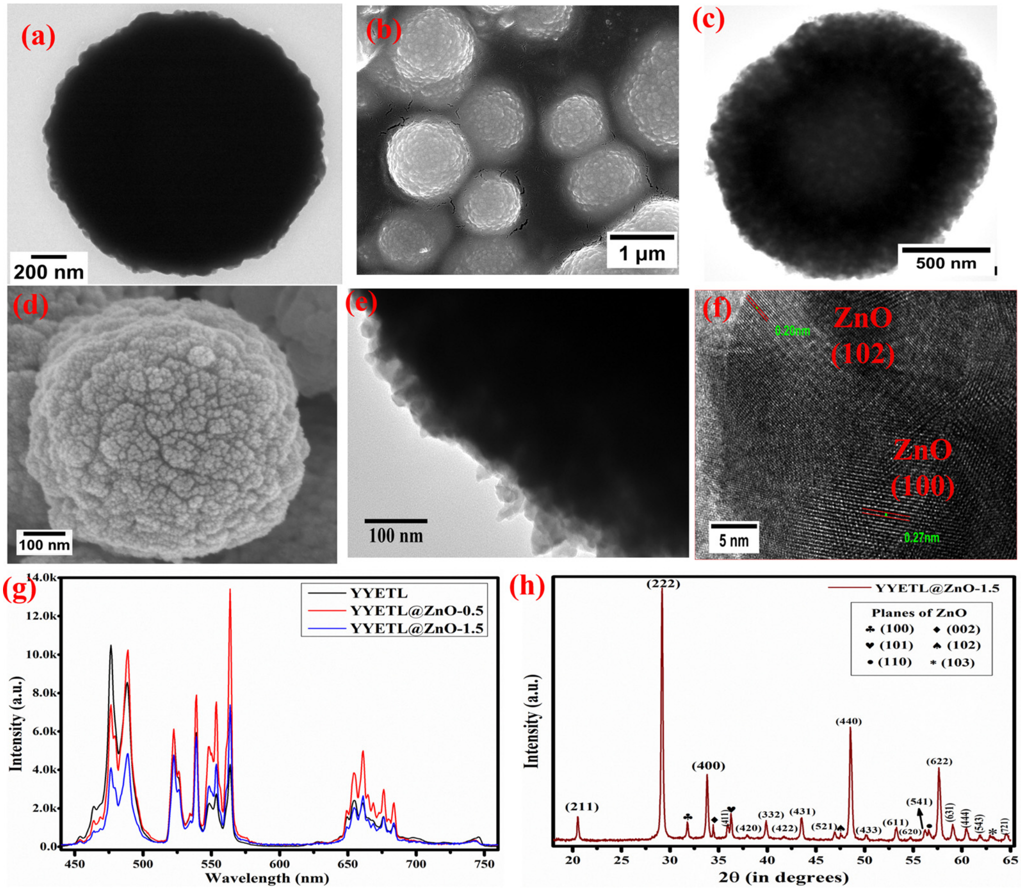

Fig. 4 FESEM, TEM, and HRTEM images of YYETL-ZnO-III-*x* microspheres for (a and b) 0.5 ml, (c)–(f) 1.5 ml of ZnO shell growth, (g) UCPL spectra of YYETL@ZnO-III-*x* microspheres and (h) XRD pattern of YYETL@ZnO-1.5 core–shell microspheres.

The FESEM image (Fig. 4b) of the YYETL@ZnO-III-0.5 microspheres depicts a rough surface after coating of a thin ZnO layer onto the core microspheres. TEM images (Fig. 4c and e and Fig. S1a–c in the SI) of the YYETL@ZnO-III-1.5 microspheres show an increase in the thickness of the deposited shell, as well as the appearance of loose nanostructures in the solution for 1.5 ml of precursor solution used in ZnO shell growth. No contrast in the core and shell materials is seen due to the high density, large size, and thickness of the synthesized YYETL@ZnO core–shell microspheres in the μm range. The FESEM image of the YYETL@ZnO-1.5 microspheres in Fig. 4(d) shows a further increase in surface roughness after thick ZnO layer deposition. The HRTEM image of the YYETL@ZnO-1.5 microspheres in Fig. 4(e) shows the lattice fringes of the shell with an interplanar spacing of 0.20 nm and 0.27 nm, which can be indexed to the (102) and (100) planes of ZnO. The HAADF-STEM 2D image of a YYETL@ZnO-1.5 microsphere and its elemental mapping are shown in Fig. S2 in the SI. Throughout the core–shell microspheres, a uniform distribution of yttrium, oxygen, zinc, ytterbium, erbium, and thulium elements is seen, which thereby confirms the presence of all the elements. The XRD pattern (Fig. 4g) of the YYETL@ZnO-III-1.5 heterostructure depicts planes corresponding to Y_2O_3 (JCPDS card no. 25-1200) and ZnO (JCPDS card no. 36-1451). Due to the relatively low concentration of doped lanthanide ions and lithium ions and their effective substitution at the host metal cation site, we do not see their oxide peaks in the XRD spectra.[34] UCPL spectra (Fig. 4g) of YYETL and YYETL@ZnO-III-x microspheres under 975 nm laser excitation depict the impact of ZnO shell growth on the upconversion emission process.[12] The intensity of anti-Stokes' emission increases after the initial coating of 0.5 ml of ZnO layer. This could be due to the passivation of surface defects and insulation of the YYETL phosphor core from its environment.[35] The growth of a heterostructure in a core–shell design prevents leakage of rare earth ions from the core due to electrostatic repulsion and the inability to occupy the divalent sites of Zn^{2+} in ZnO.[36] The anti-Stokes emission is quenched for 1.5 ml of ZnO shell growth due to the loss of energy to crystal defects present in the thick ZnO shell, as well as the transfer of energy *via* the radiation-reabsorption process to loose ZnO nanostructures.[30] PL of ZnO nanoparticles synthesized by the hydrothermal method is included in Fig. S3 in the SI. We observed a sharp emission in the UV region, which corresponds to the near band edge emission of ZnO. The broad peak in the visible region, between 450 and 700 nm, is due to its intrinsic defects. These defects lie within the band gap of ZnO and play a crucial role in making it responsive to visible radiation.[37] In addition, the decrease in emission could also be due to a thicker shell limiting absorption of NIR light by Yb^{3+} ions in the core. The presence of misfit strain between two lattice mismatched crystals of core and shell materials could have also negatively impacted the anti-Stokes emission.[20] For YYETL@ZnO-III microspheres synthesized *via* the interlayer mediated hydrothermal method, conformal ZnO shell growth was possible for only x = 0.5 ml because of the positive value of the tensile interfacial strain between the two crystals. For x = 1.5, ZnO nanoparticles, apart from depositing on YYETL microspheres, form anisotropic nanostructures in the reaction solution. For a thin ZnO shell, the reaction kinetics of overgrowth layer deposition are mainly governed by the Frank–van der Merwe (FM) model, which later transitions to the Stranski–Krastanov (SK) model as the shell thickness increases.[26] The misfit strain between two lattice mismatched materials induces lattice defects such as dislocations, which relax the strain at the interface and lead to the formation of free ZnO nanostructures.[38] The interaction potential of atoms/ions is anharmonic between the attractive and repulsive pairs, so the sign of lattice mismatch is expected to influence the core–shell growth.[19] Despite the large misfit strain, minimal ZnO shell growth is only allowed on the YYETL microspheres because of the positive value of the interfacial strain; otherwise, the high mismatch in lattice constants of core and shell crystals does not allow the deposition of overgrowth layer. Thus, both the magnitude and sign of lattice mismatch play a crucial role in designing the UCNPs@semiconductor core–shell heterostructure.

4. Conclusions

In summary, we have used three different methods to develop a conformal core–shell heterostructure between two lattice-mismatched crystals of YYETL and ZnO and compared the quality of the grown shell. In the interlayer conversion method, we formed an amorphous interlayer of AA-$[Zn(OH)_4]^{2-}$ to eliminate the high lattice mismatch between YYETL and ZnO crystals and thereby convert the interlayer to ZnO by thermal decomposition of $Zn(OH)_4$. This results in the formation of a thick ZnO shell with many free ZnO nanoparticles not attached to the core. The disadvantage of this method is the inability to control shell thickness and the formation of calcination-induced defects, which makes us switch to the hydrothermal method of ZnO synthesis. In the second method of hydrothermal synthesis, ZnO nanocrystals either nucleate and deposit as discrete islands on the surface of YYETL microspheres, *via* electrostatic attraction through the Volmer–Weber model of epitaxial growth or form free ZnO micro/nanostructures in solution. Therefore, to remove this discrepancy, in the interlayer mediated hydrothermal method, we have introduced PVP molecules as an interlayer between YYETL and ZnO crystals to facilitate overall shell growth on the core initially *via* the Frank-van der Merwe (FM) model and later transition to the Stranski–Krastanov (SK) model as the shell thickness increases. It also highlights the role of interfacial strain and how it allows the growth of the overlayer only up to critical thickness, as beyond it, misfit strain induces dislocation defects, resulting in the formation of free ZnO nanostructures in solution. The positive sign of the lattice mismatch indicates the existence of a tensile strain at the core–shell interface, which aids in overgrowth layer deposition up to a limited value. Among the developed synthetic strategies, the interlayer mediated hydrothermal method has been able to successfully coat a uniform layer of the ZnO shell around the core YYETL microspheres up to the critical thickness. This protocol can be used to design a series of upconversion phosphors@semiconductor core–shell heterostructures for their possible application in photovoltaics, photocatalysis, and biomedical applications like imaging and photodynamic therapy.

Conflicts of interest

There are no conflicts to declare.

Data availability

The data will be made available on reasonable request from the corresponding author.

The supplementary information contains TEM/HRTEM images as well as HAADF-STEM-EDX elemental mapping images of YYETL@ZnO-1.5 microspheres depicting the growth of ZnO shell over YYETL micorspheres. PL of ZnO nanoparticles are also provided to show the intrinsic defects present in the material. See DOI: **https://doi.org/10.1039/d5cp00156k**.

Acknowledgements

The authors thank Multifunctional Nanomaterials Lab, CSIR-NCL, Pune, and Department of Physics, Indian Institute of Technology (ISM) Dhanbad for providing research facilities for this work.

References

1 Y. Li, J. Zhang, Q. Chen, X. Xia and M. Chen, Emerging of Heterostructure Materials in Energy Storage: A Review, *Adv. Mater.*, 2021, **33**(27), 2100855, DOI: **10.1002/adma.202100855**.

2 R. Ghosh Chaudhuri and S. Paria, Core/shell nanoparticles: Classes, properties, synthesis mechanisms, characterization, and applications, *Chem. Rev.*, 2012, **112**, 2373–2433, DOI: **10.1021/cr100449n**.

3 Y. Cheng, M. Gong, T. Xu, E. Liu, J. Fan, H. Miao and X. Hu, Epitaxial Grown Sb2Se3@Sb2S3Core-Shell Nanorod Radial-Axial Hierarchical Heterostructure with Enhanced Photoelectrochemical Water Splitting Performance, *ACS Appl. Mater. Interfaces*, 2022, **14**, 23785–23796, DOI: **10.1021/acsami.2c05551**.

4 L. Jing, S. V. Kershaw, T. Kipp, S. Kalytchuk, K. Ding, J. Zeng, M. Jiao, X. Sun, A. Mews, A. L. Rogach and M. Gao, Insight into strain effects on band alignment shifts, carrier localization and recombination kinetics in CdTe/CdS core/shell quantum dots, *J. Am. Chem. Soc.*, 2015, **137**, 2073–2084, DOI: **10.1021/ja5127352**.

5 K. Sahoo, S. Ranjan and M. Kumar, Lattice-strain induced photophysical properties of NaYF4: Yb3 +, Tm3+ upconverting phosphors, *J. Lumin.*, 2022, **251**, 119249, DOI: **10.1016/j.jlumin.2022.119249**.

6 H. Peng Feng, L. Tang, G. Ming Zeng, Y. Zhou, Y. Cheng Deng, X. Ren, B. Song, C. Liang, M. Yun Wei and J. Fang Yu, Core-shell nanomaterials: Applications in energy storage and conversion, *Adv. Colloid Interface Sci.*, 2019, **267**, 26–46, DOI: **10.1016/j.cis.2019.03.001**.

7 P. Reiss, M. Protière and L. Li, Core/shell semiconductor nanocrystals, *Small*, 2009, **5**, 154–168, DOI: **10.1002/smll.200800841**.

8 Z. Luo, L. Zhang, R. Zeng, L. Su and D. Tang, Near-Infrared Light-Excited Core-Core-Shell UCNP@Au@CdS Upconversion Nanospheres for Ultrasensitive Photoelectrochemical Enzyme Immunoassay, *Anal. Chem.*, 2018, **90**, 9568–9575, DOI: **10.1021/acs.analchem.8b02421**.

9 Q. Q. Dou, A. Rengaramchandran, S. T. Selvan, R. Paulmurugan and Y. Zhang, Core-shell upconversion nanoparticle – semiconductor heterostructures for photodynamic therapy, *Sci. Rep.*, 2015, **5**, 8252, DOI: **10.1038/srep08252**.

10 Y. Li, Y. Li, Y. Bai, R. Wang, L. Lin and Y. Sun, Semiconductor ZnO based photosensitizer core-shell upconversion nanoparticle heterojunction for photodynamic therapy, *RSC Adv.*, 2020, **10**, 38416–38423, DOI: **10.1039/d0ra07466g**.

11 W. N. Wang, F. Zhang, C. L. Zhang, Y. C. Guo, W. Dai and H. S. Qian, Fabrication of Zinc Oxide Composite Microfibers for Near-Infrared-Light-Mediated Photocatalysis, *ChemCatChem*, 2017, **9**, 3611–3617, DOI: **10.1002/cctc.201700781**.

12 S. Jayswal, M. N. Luwang and R. S. Moirangthem, Tuning the optical properties of Ln^{3+}-doped-Y_2O_3@ZnO@Au core-shell heterostructures for visible-to-NIR photon harvesting, *Surf. Interfaces*, 2024, **44**, 103775, DOI: **10.1016/j.surfin.2023.103775**.

13 M. D. Wisser, M. Chea, Y. Lin, D. M. Wu, W. L. Mao, A. Salleo and J. A. Dionne, Strain-induced modification of optical selection rules in lanthanide-based upconverting nanoparticles, *Nano Lett.*, 2015, **15**, 1891–1897, DOI: **10.1021/nl504738k**.

14 G. Chen, H. Ågren, T. Y. Ohulchanskyy and P. N. Prasad, Light upconverting core-shell nanostructures: Nanophotonic control for emerging applications, *Chem. Soc. Rev.*, 2015, **44**, 1680–1713, DOI: **10.1039/c4cs00170b**.

15 C. Tan, J. Chen, X. J. Wu and H. Zhang, Epitaxial growth of hybrid nanostructures, *Nat. Rev. Mater.*, 2018, **3**, 17089, DOI: **10.1038/natrevmats.2017.89**.

16 A. M. Smith, A. M. Mohs and S. Nie, Tuning the optical and electronic properties of colloidal nanocrystals by lattice strain, *Nat. Nanotechnol.*, 2009, **4**, 56–63, DOI: **10.1038/nnano.2008.360**.

17 C. Zhang and J. Y. Lee, Prevalence of anisotropic shell growth in rare earth core-shell upconversion nanocrystals, *ACS Nano*, 2013, **7**, 4393–4402, DOI: **10.1021/nn4009214**.

18 X. Wan, Y. Pan, Y. Xu, J. Liu, H. Chen, R. Pan, Y. Zhao, P. Su, Y. Li, X. Zhang, S. Zhang, H. Li, D. Su, Y. Weng and J. Zhang, Ultralong Lifetime of Plasmon-Excited Electrons Realized in Nonepitaxial/Epitaxial Au@CdS/$CsPbBr_3$ Triple-Heteronanocrystals, *Adv. Mater.*, 2023, **35**(3), 2207555, DOI: **10.1002/adma.202207555**.

19 N. J. J. Johnson and F. C. J. M. Van Veggel, Lanthanide-based heteroepitaxial core-shell nanostructures: Compressive versus tensile strain asymmetry, *ACS Nano*, 2014, **8**, 10517–10527, DOI: **10.1021/nn503946t**.

20 C. Zhang and J. Y. Lee, Prevalence of anisotropic shell growth in rare earth core-shell upconversion nanocrystals, *ACS Nano*, 2013, **7**, 4393–4402, DOI: **10.1021/nn4009214**.

21 P. Mélinon, S. Begin-Colin, J. L. Duvail, F. Gauffre, N. H. Boime, G. Ledoux, J. Plain, P. Reiss, F. Silly and B. Warot-Fonrose, Engineered inorganic core/shell nanoparticles, *Phys. Rep.*, 2014, **543**, 163–197, DOI: **10.1016/j.physrep.2014.05.003**.

22 W. Wang, M. Zhao, C. Zhang and H. Qian, Recent Advances in Controlled Synthesis of Upconversion Nanoparticles and Semiconductor Heterostructures, *Chem. Rec.*, 2020, **20**, 2–9, DOI: **10.1002/tcr.201900006**.

23 S. Jayswal, R. S. Ningthoujam and R. S. Moirangthem, Observation of Stark splitting in micro upconversion photoluminescence spectra of polycrystalline Ln3+ doped Y2O3microspheres, *Nanotechnology*, 2022, **33**, 335702, DOI: **10.1088/1361-6528/ac6cf7**.

24 F. Zhang, W. N. Wang, H. P. Cong, L. B. Luo, Z. B. Zha and H. S. Qian, Facile Synthesis of Upconverting Nanoparticles/Zinc Oxide Core–Shell Nanostructures with Large Lattice Mismatch for Infrared Triggered Photocatalysis, *Part. Part. Syst. Charact.*, 2017, **34**(2), 1600222, DOI: **10.1002/ppsc.201600222**.

25 C. Cui, M. Tou, M. Li, Z. Luo, L. Xiao, S. Bai and Z. Li, Heterogeneous Semiconductor Shells Sequentially Coated on Upconversion Nanoplates for NIR-Light Enhanced Photocatalysis, *Inorg. Chem.*, 2017, **56**, 2328–2336, DOI: **10.1021/acs.inorgchem.6b03079**.

26 J. Liu and J. Zhang, Nanointerface Chemistry: Lattice-Mismatch-Directed Synthesis and Application of Hybrid Nanocrystals, *Chem. Rev.*, 2020, **120**, 2123–2170, DOI: **10.1021/acs.chemrev.9b00443**.

27 J. Zhang and Y. Tang, Nonepitaxial Growth of Hybrid Core-Shell Nanostructures with Large Lattice Mismatches, *Science*, 2010, 1634–1638.

28 H. Anwer and J. Park, Near-infrared to visible photon transition by upconverting NaYF$_4$: Yb^{3+}, Gd^{3+}, Tm^{3+}@Bi$_2$WO$_6$ core@shell composite for bisphenol A degradation in solar light, *Appl. Catal., B*, 2019, **243**, 438–447, DOI: **10.1016/j.apcatb.2018.10.074**.

29 M. Tou, Z. Luo, S. Bai, F. Liu, Q. Chai, S. Li and Z. Li, Sequential coating upconversion NaYF$_4$: Yb, Tm nanocrystals with SiO$_2$ and ZnO layers for NIR-driven photocatalytic and antibacterial applications, *Mater. Sci. Eng. C*, 2017, **70**, 1141–1148, DOI: **10.1016/j.msec.2016.03.038**.

30 X. Guo, W. Song, C. Chen, W. Di and W. Qin, Near-infrared photocatalysis of β-NaYF$_4$:Yb^{3+},Tm^{3+}@ZnO composites, *Phys. Chem. Chem. Phys.*, 2013, **15**, 14681–14688, DOI: **10.1039/c3cp52248b**.

31 K. M. Koczkur, S. Mourdikoudis, L. Polavarapu and S. E. Skrabalak, Polyvinylpyrrolidone (PVP) in nanoparticle synthesis, *Dalton Trans.*, 2015, 17883–17905, DOI: **10.1039/c5dt02964c**.

32 C. Cui, M. Tou, M. Li, Z. Luo, L. Xiao, S. Bai and Z. Li, Heterogeneous Semiconductor Shells Sequentially Coated on Upconversion Nanoplates for NIR-Light Enhanced Photocatalysis, *Inorg. Chem.*, 2017, **56**, 2328–2336, DOI: **10.1021/acs.inorgchem.6b03079**.

33 M. Tou, Z. Luo, S. Bai, F. Liu, Q. Chai, S. Li and Z. Li, Sequential coating upconversion NaYF$_4$: Yb, Tm nanocrystals with SiO$_2$ and ZnO layers for NIR-driven photocatalytic and antibacterial applications, *Mater. Sci. Eng. C*, 2017, **70**, 1141–1148, DOI: **10.1016/j.msec.2016.03.038**.

34 H. M. Noh, J. H. Oh, J. H. Jeong, S. H. Park and B. C. Choi, White upconversion emission and color tunability of Y$_2$O$_3$:R(R = Yb^{3+}, Er^{3+}, Tm^{3+}) nanophosphors, *Curr. Appl. Phys.*, 2022, **39**, 190–195, DOI: **10.1016/j.cap.2022.05.002**.

35 Q. Su, S. Han, X. Xie, H. Zhu, H. Chen, C. Chen, R. Liu, X. Chen, F. Wang and X. Liu, The Effect of Surface Coating on Energy Migration-Mediated Upconversion, *J. Am. Chem. Soc.*, 2012, **134**(51), 20849–20857, DOI: **10.1021/ja3111048**.

36 Y. Wang, L. Sun, J. Xiao, W. Feng, J. Zhou and J. Shen, Rare-Earth Nanoparticles with Enhanced Upconversion Emission and Suppressed Rare-Earth-Ion Leakage, *Nanoscale*, 2012, 5558–5564, DOI: **10.1002/chem.201103485**.

37 S. Nadupalli, S. Repp, S. Weber and E. Erdem, About defect phenomena in ZnO nanocrystals, *Nanoscale*, 2021, **13**, 9160–9171, DOI: **10.1039/d1nr00943e**.

38 J. Zhao, B. Chen and F. Wang, Shedding Light on the Role of Misfit Strain in Controlling Core–Shell Nanocrystals, *Adv. Mater.*, 2020, **32**(46), 2004142, DOI: **10.1002/adma.202004142**.